Article:

eprints@whiterose.ac.uk
https://eprints.whiterose.ac.uk/

Electronic materials

Optimisation of the Zr:Ti ratio in bulk lead zirconate titanate for templated grain growth using BaTiO₃ seeds

Edoardo F. Mantheakis[1,*] (iD), Beecher H. Watson III[2], Michael J. Brova[2], Gary L. Messing[2], Laura A. Stoica[3], and Ian M. Reaney[1]

[1] *Department of Material Science and Engineering, University of Sheffield, Sheffield S1 3JD, UK*

[2] *Department of Materials Science and Engineering & Materials Research Institute, Pennsylvania State University, University Park, PA 16802, USA*

[3] *Thales UK, 350 Longwater Avenue, Reading RG2 6GF, UK*

ABSTRACT

Presented here is a proof of concept demonstration of the templated grain growth (TGG) process for the development of $[001]_c$ fibre-textured $Pb(Zr_xTi_{1-x})O_3$ (PZT) ceramics. $BaTiO_3$ platelets (5 and 10 vol.%) were selected to seed growth of highly oriented PZT grains resulting in texture fractions as high as 94%. The TGG process in PZT was observed to be critically dependent upon the addition of excess PbO liquid phase and may be driven by $BaTiO_3$ dissolution into the matrix. Solid solution incorporation of $BaTiO_3$ during sintering resulted in a structural shift away from the PZT morphotropic phase boundary (MPB) and a decrease in Curie temperature (T_C) by ~ 40 °C which still exceeded > 300 °C. Modification of the Zr:Ti ratio in untextured ceramic analogues was explored as a strategy to tailor dielectric, ferroelectric, and electromechanical properties. An initial PZT matrix composition of $Pb(Zr_{0.56}Ti_{0.44})O_3$ resulted in a final bulk $Pb_{0.947}Ba_{0.053}(Zr_{0.531}Ti_{0.469})O_3$ ceramic having MPB-like properties of $d_{33} = 453$ pC/N, tan δ = 0.017, $T_C = 340$ °C, and $E_c = 9.3$ kV/cm, which was observed to be similar to commercial 'soft' PZT-5A1.

Introduction

Since the inception and development of $Pb(Zr_xTi_{1-x})O_3$ (PZT) perovskite solid solutions [1–5], PZT has been extensively explored as a model piezoelectric material with renewed focus into the origins of piezoelectricity [6–8]. The maximum piezoelectric response is found near the morphotropic phase boundary (MPB) at $x \sim 0.52$ [9]. Compositional modification by aliovalent substitution of donor and/or acceptor dopant ions on both A- and B-sites in the perovskite structure is extensively documented for tailoring of piezoelectric properties [9, 10]. Donor-doped PZT or 'soft' PZT ceramics, commonly with La^{3+} on the A-site (PLZT) and Nb^{5+} on the B-site

Springer

(PNZT), are generally characterised by greater polarisation, piezoelectric coefficients ($d_{33} > 600$ pC/N), and dielectric losses (tan δ) through increased extrinsic domain wall contributions primarily underpinned by suppression of the Curie temperature (T_C) [11]. 'Hard' PZT ceramics, where acceptor dopants introduce domain wall pinning defects, exhibit decreased piezoelectric activity ($d_{33} < 300$ pC/N), reduced tan δ from suppressed extrinsic effects, along with large coercive fields (E_c) and relatively high T_C suitable for high drive applications [12].

In the last few decades, there have been numerous efforts to push the limits of electromechanical properties, namely through development of binary $Pb(Zn_{1/3}Nb_{2/3})O_3$-$PbTiO_3$ (PZN-PT)[13] and $Pb(Mg_{1/3}Nb_{2/3})O_3$-$PbTiO_3$ (PMN-PT)[14] as well as ternary $Pb(Mg_{1/3}Nb_{2/3})O_3$-$PbZrO_3$-$PbTiO_3$ (PMN-PZT)[15] and $Pb(In_{1/2}Nb_{1/2})O_3$-$Pb(Mg_{1/3}Nb_{2/3})O_3$-$PbTiO_3$ (PIN-PMN-PT)[16] single crystals with very high $d_{33} > 1500$ pC/N. Textured ceramics produced by templated grain growth (TGG) with the same composition as reported single crystals have also been developed with high d_{33} coefficients approaching 1000 pC/N [17, 18]. Textured ceramics provide a pathway to harness the effects of piezoelectric anisotropy while engineering the microstructure to tailor the piezoelectric properties of these materials [19]. Despite the strong enhancements in electromechanical behaviour through controlling crystallographic anisotropy, many of the existing materials to date are limited by low-temperature rhombohedral–tetragonal phase transitions ($T_{r-t} < 150$ °C), low Curie temperatures ($T_C < 230$ °C), and small coercive fields ($E_c < 9$ kV/cm) which risk depoling as a result of temperature rises from heat generation or high drive fields [20].

PZT provides an advantage with greater coercive fields ($E_c > 10$ kV/cm) and high Curie temperatures ($T_C > 230$ °C) to mitigate the risk of depoling in transducers. Incongruent melting across the whole PZ-PT solid solution range [21] has presented a substantial challenge in the development of PZT single crystals [22], commonly resulting in significant compositional segregation, crystal size limitations, and twinning defects. The literature on developments in textured PZT ceramics is limited to tape casting and hot pressing of PZT powders with cubic morphology [23] or tape casting of PZT powder with a large volume fraction (~ 40 vol.%

of < 111 > oriented $Ba_6Ti_{17}O_{40}$) of seeds [24]. In all cases, achieved texture fractions were low ($f < 60\%$), but all authors noted that excess PbO played a critical role in promoting textured grain growth. The use of heterogenous seed crystals in TGG requires strict selection criteria: similar crystal structure with minimised lattice mismatch, sufficient chemical stability to survive the epitaxy process, and an understanding of the effect of the seed as a composite system within the host material [25]. Whilst there is significant published work on Ba- [26] and Sr-doped PZT [27] with varying dopant levels across the whole solid solution range, there is minimal literature on the effect of fixed low-level inclusions varying the PZT Zr:Ti ratio, representative of TGG. The addition of dopants necessitates the modification of the Zr:Ti to compensate for seed chemistry to retain a near MPB composition with optimised piezoelectric properties.

This work lays out critical factors in the development of grain-oriented PZT ceramics utilising platelet-shaped $BaTiO_3$ seeds and demonstrates a proof of concept for texturing PZT. The effects of $BaTiO_3$ seeds in the microstructure are explored and the relationship between the PZT matrix composition and resulting piezoelectric properties are established.

Methodology

Fabrication of textured ceramics

The matrix compositions selected for this investigation were a PZT powder synthesised in-house (referred to simply as PZT) and a commercial powder designated PZT-5A1 (Morgan Technical Ceramics, UK). PZT powder was synthesised from mixed metal oxides of PbO (99.9% purity, Alfa Aesar), ZrO_2 (99% purity, Sigma-Aldrich), and TiO_2 (rutile, $\geq$ 99.9% purity, Sigma-Aldrich). Oxide powders were blended by vibratory milling together in isopropanol in a 1 L Nalgene bottle with 350 g of a 1:1:1 mass ratio of 3, 5, and 10 mm diameter YSZ milling media spheres for 72 h, dried overnight, sieved to remove any agglomerates, and calcined at 800 °C for 2 h. The PZT powder was re-milled for 72 h to break up aggregates that formed during calcination. PZT-5A1 was similarly prepared by vibratory milling for 72 h. Inspection of the as-milled powders, shown in Fig. 1, revealed particles sizes below 1 μm. Both in-house synthesised PZT and PZT-5A1 material were studied

to give an insight into whether TGG of PZT is possible based on the controlled preparation of PZT material and in compositions with dopant elements that may affect textured microstructure evolution.

Fibre-textured PZT ceramics with $[001]_c$ preferred orientation were seeded using 5 vol.% $BaTiO_3$ templates (Entekno Materials, Turkey) (Fig. 2) that have a platelet morphology as shown in Fig. 3 [28]. $[001]_c$ oriented PZT-5A1 ceramics were seeded using 10 vol.% $BaTiO_3$ platelets. Commercial PZT powders commonly include liquid phase formers to aid densification during sintering. The exact quantity of liquid phase former present in the PZT-5A1 powder is not disclosed by the manufacturer; therefore, the inclusion of an increased vol.% of $BaTiO_3$ platelets is theorised to promote initial textured grain epitaxy at the known detriment of late stage textured grain impingement. PZT slurries (56 vol.% solids loading) with 5 vol.% $BaTiO_3$ seeds with platelet morphology had excess PbO (5 wt.%) added to facilitate grain growth during TGG. Slurries made with PZT-5A1 and 10 vol.% $BaTiO_3$ platelets contained no added PbO excess. All slurries were formed using an aqueous binder system (WB4101, Polymer Innovations, USA), mixed using a speed mixer at 1200 rpm for 20 min, and tape cast using a doctor blade setup with a gap height of 200 μm. Dried tapes were sectioned, stacked, and uniaxially laminated under an applied pressure of 15 MPa at 75 °C, then hydrostatically laminated at 200 MPa at 75 °C for 20 min. Organic binders were burnt out by heating at 0.1 °C/min to 350 °C and holding for 9 h, followed by heating to 450 °C and holding for 5 h. Green bodies were enclosed in covered alumina crucibles with $PbZrO_3$ (PZ) + 5 wt.% ZrO_2 sacrificial powder to ensure controlled PbO loss, and heated at 5 °C/min
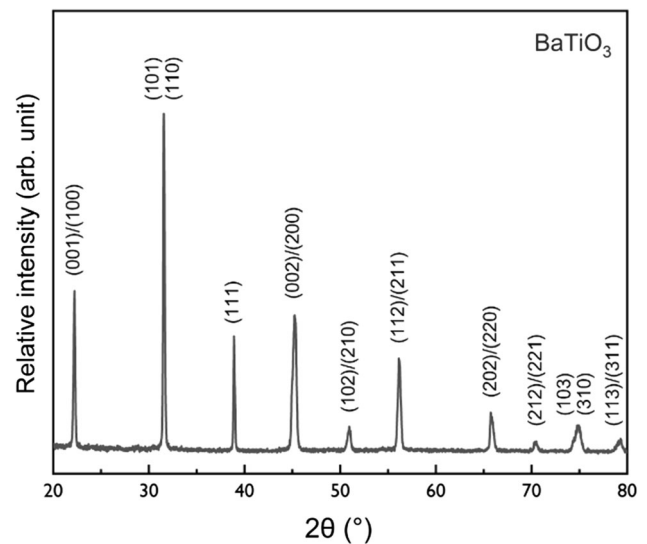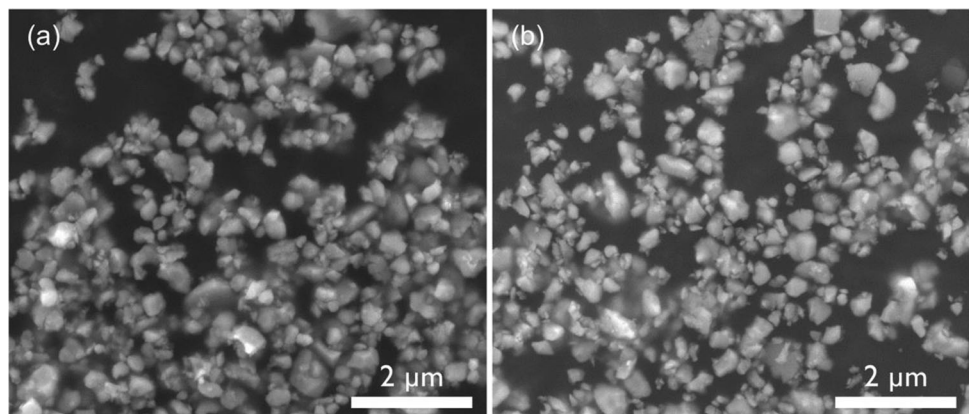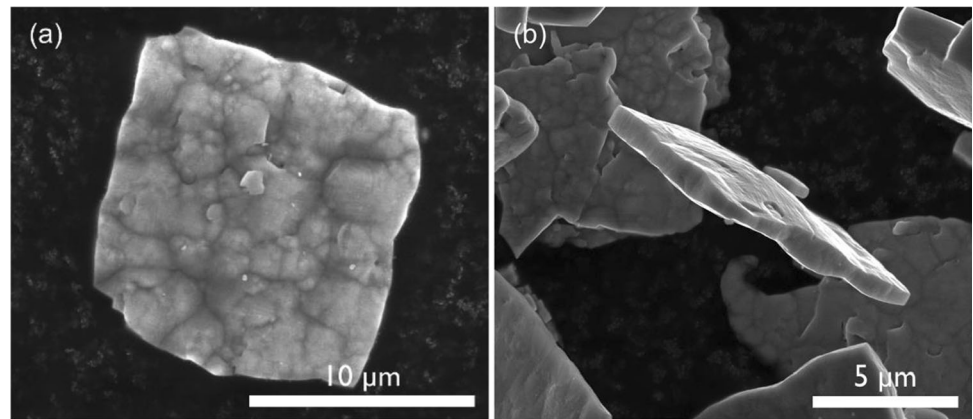

Figure 2 XRD pattern for platelet-shaped $BaTiO_3$ seeds.

to 1250 °C for 2, 4, and 8 h holds to investigate textured microstructure evolution.

Fabrication of untextured ceramics

Randomly oriented $Pb_yBa_{1-y}(Zr_zTi_{1-z})O_3$ specimens, with calcined powder compositions ranging from an undoped MPB composition $x = 0.52$ to $x = 0.61$ with fixed 5 vol.% $BaTiO_3$ additions, were synthesised by a conventional solid-state route using PbO (99.9% purity, Alfa Aesar), ZrO_2 (99% purity, Sigma-Aldrich), TiO_2 (rutile, $\geq$ 99.9% purity, Sigma-Aldrich), and $BaTiO_3$ (Entekno Materials, Turkey). Powder regents were ball milled together in isopropanol for 24 h, dried overnight, sieved to remove any agglomerates, and calcined at 800 °C for 2 h. The calcined PZT powder was re-milled with 5 vol.% $BaTiO_3$ platelets and 10 wt.% PVA binder solution for

Figure 1 SE images of (**a**) in-house PZT and (**b**) commercial PZT-5A1 particles after vibratory milling for 72 h.

Figure 3 SE images of a platelet-shaped BaTiO₃ seed (**a**) flat facing and (**b**) edge facing.

24 h. Green bodies were uniaxially pressed at 125 MPa, with the BaTiO₃ platelets, destroyed during milling, randomly aligned within the pressed samples. The pressed bodies were subsequently enclosed with PZ + 5 wt.% ZrO₂ sacrificial powder during sintering. Initial binder burnout, heating at 0.1 °C/min to 550 °C and holding for 3 h, was followed by heating at 5 °C/min to 1250 °C for 2 h. The final calculated Zr concentration after the addition of BaTiO₃ is quoted to distinguish individual specimens.

Structural and microstructural characterisation

The structure and orientation of synthesised multilayers were examined using a D2 PHASER x-ray diffractometer (Bruker) operating in Bragg–Brentano geometry with Cu K_α radiation source (λ = 1.5408 Å), fitted with 2.5° Soller slits, 1 mm divergence slit, and 0.5 and 2.5 mm Ni filters to remove Cu K_β radiation. Samples were analysed between the 2θ range of 20–80°, using a step size of 0.02° and rate of 0.4°/sec. Lotgering factors were obtained by comparing the relative peak intensities with those of a randomly oriented powder XRD spectrum to quantify the degree of orientation in the multilayer samples [29].

Powder x-ray diffraction data to elucidate the crystal structure and lattice parameters of crushed pellets mixed with Si standard reference material (SRM 640d, NIST) was obtained using a STOE STADI P (CuPSD) x-ray diffractometer (STOE & Cie. GmbH) operating in transmission geometry with a monochromated Cu K_α radiation source, fitted with

6 mm divergence and detector slits. Samples were analysed between the 2θ range of 20–80°, using a step size of 0.02°. Standard x-ray tube working conditions were 40 kV and 40 mA.

Ceramic sample densities were measured via the Archimedes method to qualify the sintering parameters in fabricating samples suitable for electric characterisation. Multilayer fracture surfaces and polished untextured ceramics were examined by scanning electron microscopy (SEM, Inspect F, FEI) to investigate grain structure and morphology. The average grain size for untextured specimens was calculated using the linear intercept method [30].

Electrical characterisation

The dielectric behaviour of ceramic samples was analysed from capacitance and tan δ values measured at 1 kHz up to 500 °C using an E4980A Precision LCR meter (Agilent Technologies Inc.). Rhombohedral–tetragonal phase transition temperatures (T_{r-t}) were determined from the minimum of the second derivative plots of capacitance with respect to temperature in the low-temperature regime. Curie temperatures (T_C) were determined from first derivative plots when the derivative equals zero. Au-electroded specimens were poled at 180 °C under an applied field of 4 kV/mm for 30 min. Quasi-static d_{33} was measured at a frequency of 100 Hz using a Berlincourt PM300 d_{33} Piezometer (Piezotest Pte. Ltd), and large signal bipolar polarisation and strain hysteresis data was collected from an aixACCT TF Analyzer (aixACCT Systems GmbH).

Results and discussion

X-ray diffraction of $[001]_c$ oriented PZT multilayers

XRD patterns for fired $Pb(Zr_{0.52}Ti_{0.48})O_3$ ceramics are shown in Fig. 4(a). Randomly oriented undoped PZT ceramics have a tetragonal perovskite structure as indicated by the significant splitting in (002)/(200) peaks at 43° and 45° 2θ. All patterns are absent of any detectable PbO or pyrochlore secondary phases. When the green bodies are seeded with $BaTiO_3$ templates, the relative intensities of (00 l) reflections increase substantially by 2 h. The suppression of all (hkl) peak intensities apart from (00 l) reflections indicates an achievement of perovskite c-axis fibre texture along the $[001]_c$ direction. The Lotgering factor of $f_{(001)} = 0.91$ for PZT after 2 h increases marginally to $f_{(001)} = 0.94$ after 8 h. The XRD pattern of untextured PZT-5A1 in Fig. 4(b) indicates that the structure is less tetragonal than undoped PZT in Fig. 4(a) as seen by the decreased (001)/(100) and (002)/(200) peak splitting at 22° and 45° 2θ, respectively. After sintering for 2 h, a slight shoulder peak is visible on the (001) and (002) reflections at 22° and 45° 2θ, which is indicative of the tetragonal structure of the $BaTiO_3$ perovskite seeds. With continued heating, the shoulder peak disappears suggesting $BaTiO_3$ enters into solid solution with the PZT matrix. In this case, $BaTiO_3$ seeds can be considered to act as an isovalent dopant, with Ba^{2+} substituting Pb^{2+} on the A-site and excess Ti^{4+} shifting the Zr:Ti ratio of the bulk composition towards the tetragonal side of the MPB. It is therefore necessary to explore a suitable starting Zr:Ti ratio to compensate for $BaTiO_3$ seeding and so that ultimately a composition closer to the MPB may be achieved in textured samples.

Microstructural characterisation of $[001]_c$ oriented PZT multilayers

SEM images of fractured multilayer surfaces are shown in Fig. 5. Clear inhomogeneity in the grain microstructures is apparent in all textured specimens, the degree of which differs between undoped PZT and PZT-5A1. When sintered for 2 h at 1250 °C, the PZT microstructure is composed of large anisotropically shaped grains with 10–20 μm pores dispersed amongst a matrix of finer sized 5–10 μm equiaxed grains. The presence of elongated porosity and the absences of significant Z-contrast in the back scattered electron images suggests that $BaTiO_3$ is not thermally stable within the PZT matrix at temperatures > 1200 °C. Coarse grains > 20 μm may originate from heteroepitaxial nucleation on the (00 l) $BaTiO_3$ crystal faces prior to their dissolution in the PZT sample, whereas the PZT-5A1 microstructure shows an initial textured layer surrounding remnant porosity. The size difference between textured grains and fine equiaxed matrix grains earlier in the firing cycle, highlighted in Figs. 5(a, c), provides sufficient driving force for continued textured grain growth via
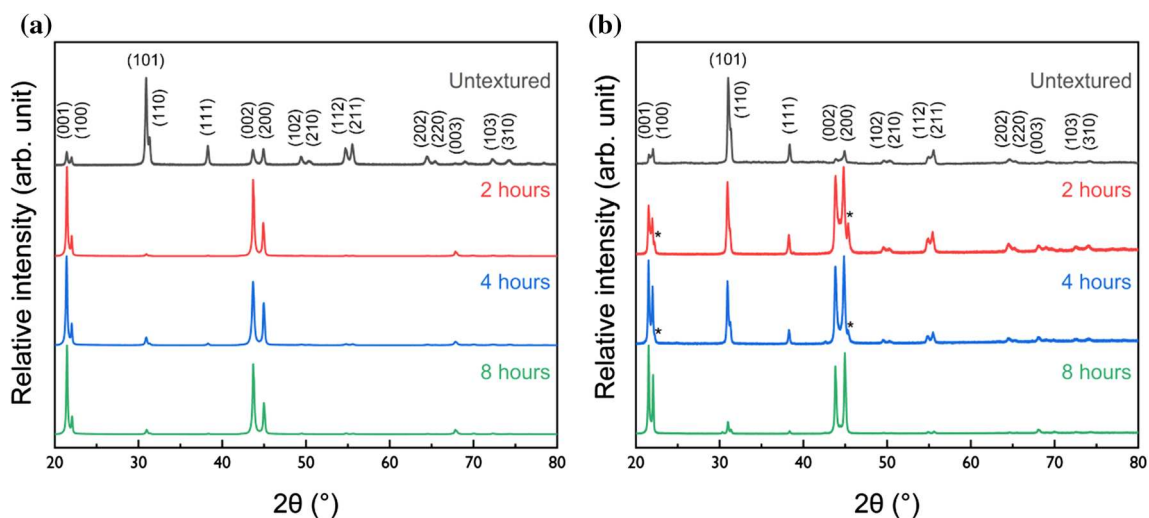
Figure 4 XRD patterns for (a) untextured PZT reference and $[001]_c$ oriented PZT multilayers (5 vol.% $BaTiO_3$) with varying sintering times; and (b) untextured PZT-5A1 reference and $[001]_c$ oriented PZT-5A1 multilayers (10 vol.% $BaTiO_3$). * Denotes secondary phase peaks.

Figure 5 SEM images of undoped PZT multilayer fracture surfaces after sintering for (**a**) 2 h and (**b**) 8 h. Fracture surfaces of PZT-5A1 multilayers after sintering for (**c**) 2 h and (**d**) 8 h.
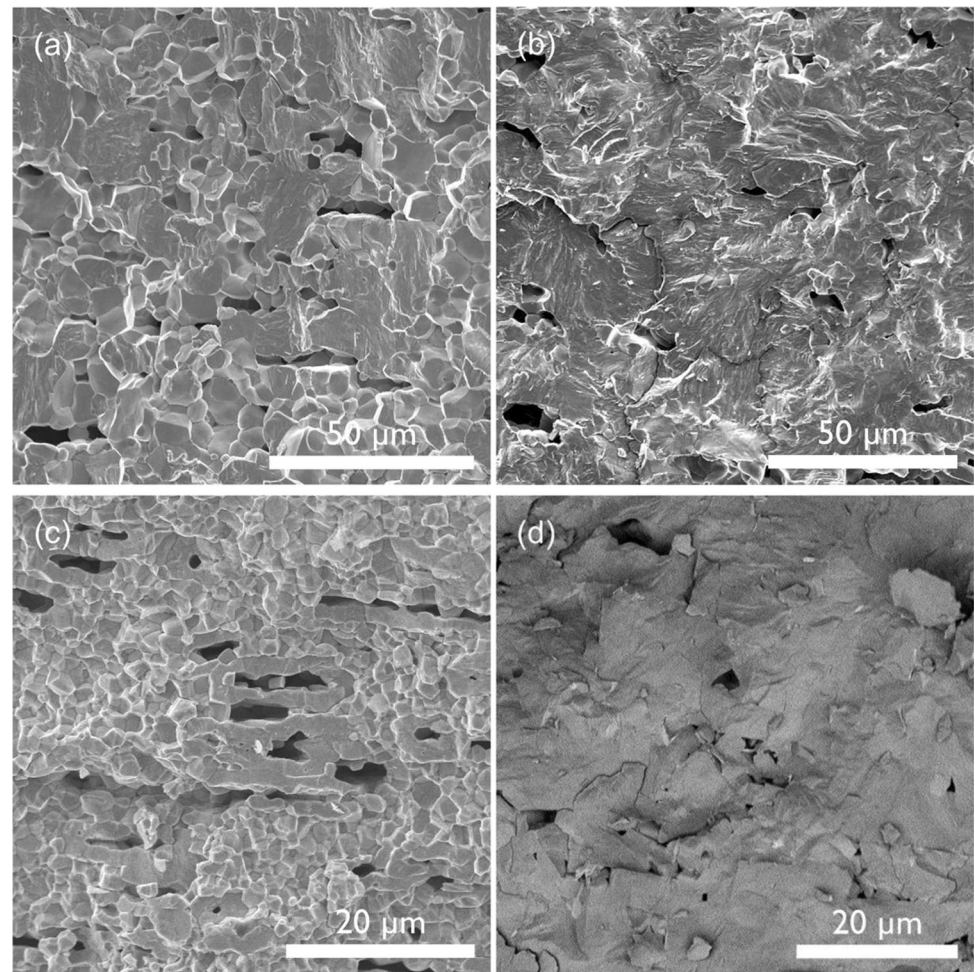
Ostwald ripening [31]. After 8 h, for both undoped PZT and PZT-5A1, a coarse grained microstructure is achieved as seen in Figs. 5(b, d).

The final densities of $\sim$ 90% theoretical resulting from the large remnant porosity indicate that more work is needed to improve the processing of BaTiO$_3$-seeded PZT ceramics. Greater control of PbO liquid phase concentration and distribution, matrix particle size/template size ratio, and employment of a pre-densification step may be required to obtain specimens suitable for piezoelectric measurements. Moreover, the large structural deviation from the MPB region as a result of the dissolution of BaTiO$_3$ seeds should be taken into consideration when tailoring compositions for maximum strain behaviour. The following sections therefore focus on providing a stronger understanding of how the Zr:Ti matrix ratio

of seeded compositions influences structure and properties.

X-ray diffraction of ceramic PZT with 5 vol.% BaTiO$_3$ seeds

XRD patterns for Pb$_y$Ba$_{1-y}$(Zr$_z$Ti$_{1-z}$)O$_3$ compositions within the range $0.49 \leq z \leq 0.58$, are shown in Fig. 6, along with calculated lattice parameters in Fig. 7. Undoped PZT ceramics, with a nominal MPB composition of $x = 0.52$, have been reported to show significant phase coexistence between tetragonal *P4mm* and rhombohedral *R3m* ferroelectric phases when synthesised via solid-state methods [32] due to each structure being near-energetically degenerate [33]. XRD patterns for samples with compositions $0.49 \leq z \leq 0.52$ were indexed according to a single tetragonal perovskite structure, with distinct
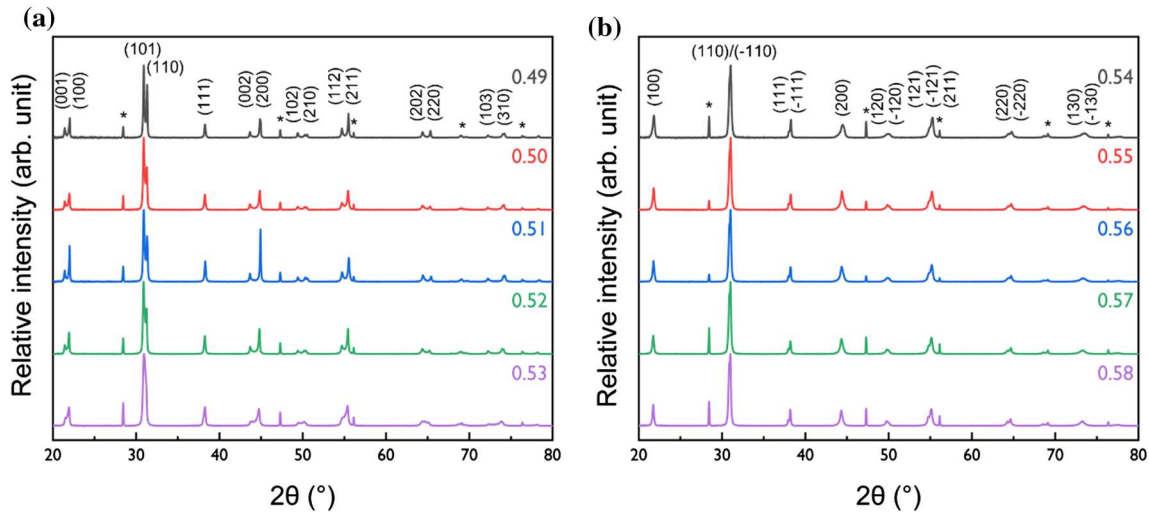
Figure 6 XRD patterns for $Pb_yBa_{1-y}(Zr_zTi_{1-z})O_3$ with Zr concentration (**a**) $z = 0.49 \leq z \leq 0.53$ and (**b**) $z = 0.54 \leq z \leq 0.58$. * Denotes Si standard peaks.
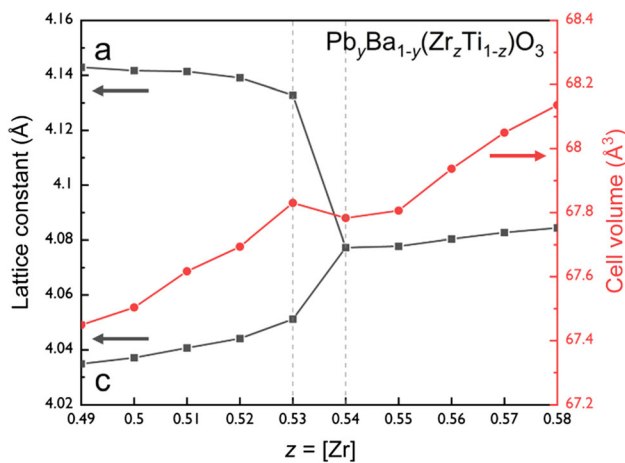

Figure 7 Calculated lattice parameters and cell volume with respect to increasing Zr concentration.

differences in c/a lattice parameters and an absence of secondary phase tetragonal peaks suggesting that the $BaTiO_3$ seeds have dissolved within the PZT matrix. Increasing the initial Zr:Ti ratio results in a decrease in 2θ spacing between tetragonal $(00\,l)_t/(h00)_t$ peak doublets until the appearance of a rhombohedral $(00\,l)_r$ singlet peak indicating phase coexistence at $z = 0.53$. XRD patterns from compositions $0.54 \leq z \leq 0.58$ show $(00\,l)_r$ singlet peaks consistent with a rhombohedral structure. The effect of Ba^{2+} substitution (R_{Ba} 1.61 Å) with a larger 12-coordinated ionic radius than Pb^{2+} (R_{Pb} 1.49 Å)[34] on the A-site as well as additional Ti^{4+} incorporation explains why the rhombohedral boundary of the MPB region is

shifted from the expected Zr:Ti ratio from 0.52:0.48 to 0.54:0.46.

Microstructural characterisation of ceramic PZT with 5 vol.% $BaTiO_3$ seeds

All untextured ceramic samples synthesised via the conventional solid-state route were found to have densities $\geq 95\%$ theoretical. Figure 8 shows the grain microstructure and morphology of bulk specimens. No continuous pore channels can be observed, with only isolated pores along grain boundaries and triple points present. The grain morphologies are distinctly equiaxed. The appearance of certain large voids > 5 μm may be due to the dissolution of broken $BaTiO_3$ template particles during sintering, similar to that seen in the textured ceramics in Fig. 5(c).

The lack of contrast in the BSE image in Fig. 8(b), excluding pores, suggests incorporation of Ba^{2+} throughout the PZT matrix and no remnant $BaTiO_3$ grains. The average grain size calculated for untextured ceramics specimens was 9 μm.

Dielectric behaviour of ceramic PZT with 5 vol.% $BaTiO_3$ seeds

The room temperature relative permittivity (ε_r), tan δ, T_C, and T_{r-t} values are shown in Fig. 9. Figure 10 shows the temperature dependencies of ε_r and tan δ for both tetragonal and rhombohedral compositions.

Comparison with undoped MPB PZT, where $x = 0.52$, indicates that ~ 5 vol.% seeds depress the

Figure 8 (**a**) SE and (**b**) BSE image of bulk untextured $Pb_yBa_{1-y}(Zr_zTi_{1-z})O_3$ microstructure.
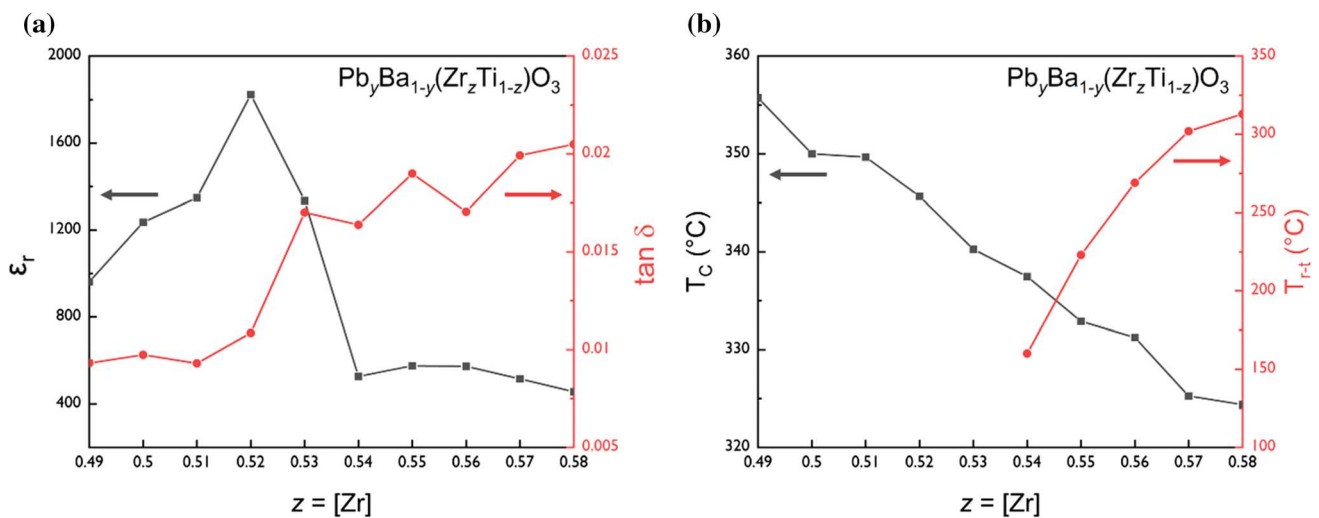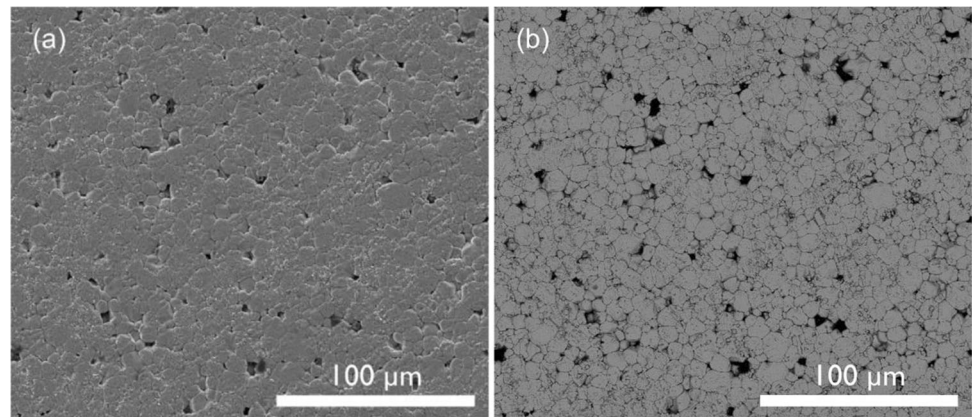
Figure 9 (**a**) Room temperature ε_r and tan δ and (**b**) T_C and T_{r-t} with respect to Zr concentration.

T_C by ∼ 40 °C. This agrees with trends seen in other studies on Ba-doped PZT across the whole solid solution range [35]. T_C also decreases with increasing Zr:Ti ratio, from 356 to 324 °C for $0.49 \leq z \leq 0.58$. The increase in ε_r on the tetragonal side can be attributed to increased contributions of ferroelectric domain wall vibrations as the bulk composition approaches the MPB. The maximum ε_r just on the tetragonal side of the MPB agrees with the previous literature on PZT [9]. There is a marked drop in ε_r for $0.52 \leq z \leq 0.54$ which continues across the MPB into the rhombohedral phase field.

All rhombohedral compositions show a secondary dielectric anomaly identified as a rhombohedral–tetragonal phase transition (T_{r-t}) which increases in temperature with increasing Zr:Ti ratio in Fig. 10(c). The T_{r-t} first appears in the composition $z = 0.54$

which agrees with the lattice structure characterisation that indicates this is the rhombohedral side of the MPB region. Since the $z = 0.54$ composition is so closely situated near the MPB region, the energy required to induce a rhombohedral–tetragonal structural distortion is at a minimum and results in a T_{r-t} of 160 °C. As the structure becomes increasingly rhombohedral with increasing Zr concentration from $z = 0.54$ to $z = 0.58$, the T_{r-t} increases up to 313 °C following the trend representative of many relaxor-based $PbTiO_3$ materials on the rhombohedral side of the MPB [36]. The trend in T_{r-t} is also reflected in the tan δ data in Fig. 10(d) as structural distortions in the perovskite unit cell near the T_{r-t} phase transition temperatures contribute to changes in unit cell polarisation and dielectric losses.
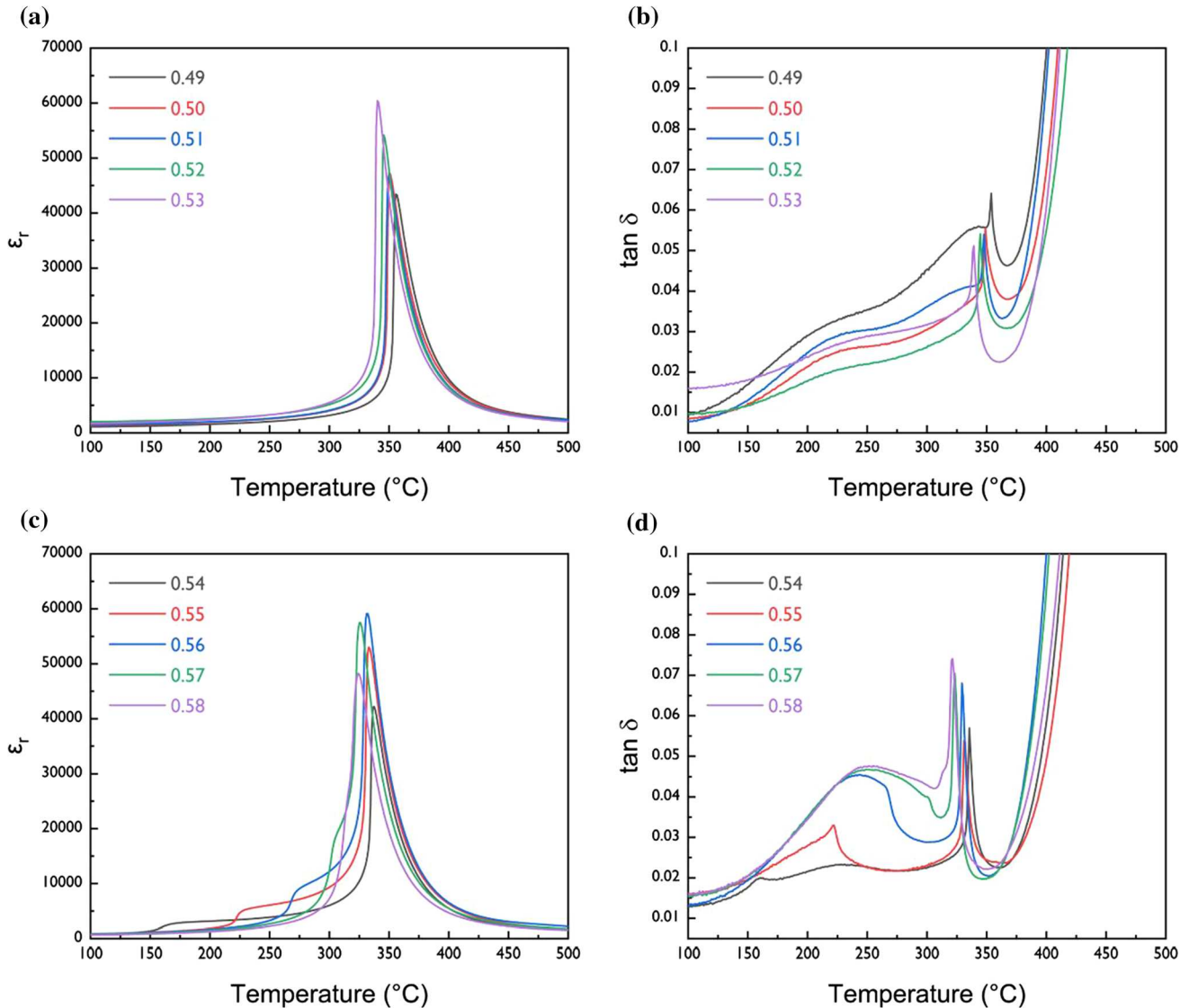
Figure 10 (**a**, **c**) Temperature dependenence of ε_r and (**b**, **d**) tan δ for tetragonal $0.49 \leq z \leq 0.53$ and rhombohedral $0.54 \leq z \leq 0.58$ compositions with general formula $Pb_yBa_{1-y}(Zr_zTi_{1-z})O_3$.

Ferroelectric hysteresis of ceramic PZT with 5 vol.% BaTiO₃ seeds

Figure 11 shows polarisation hysteresis and strain hysteresis loops for PZT ceramic samples with the optimum composition $z = 0.53$ and PZT-5A1. Both the optimised composition and PZT-5A1 exhibit squared ferroelectric polarisation loops and 'butterfly' strain loops. Saturation, P_s, and remnant, P_r polarisation values for $z = 0.53$ ($P_s = 41.8$ μC/cm², $P_r = 37.1$ μC/cm²) are comparable to the PZT-5A1 specimen ($P_s = 43.1$ μC/cm², $P_r = 34.1$ μC/cm²). The E_c for the $z = 0.53$ composition is slightly decreased at

9.3 kV/cm compared to PZT-5A1 variant at 9.7 kV/cm because the energy barrier to ferroelectric switching is observed to be lower on the rhombohedral side of the MPB than on the tetragonal side. Strain-field data give a maximum strain, S_{max}, of 0.25% for $x = 0.53$.

Piezoelectric properties

Quasi-static Berlincourt d_{33} measurements are shown in Fig. 12. Piezoelectric charge coefficients show a general improvement compared to conventional undoped PZT. There is an increase in d_{33} moving
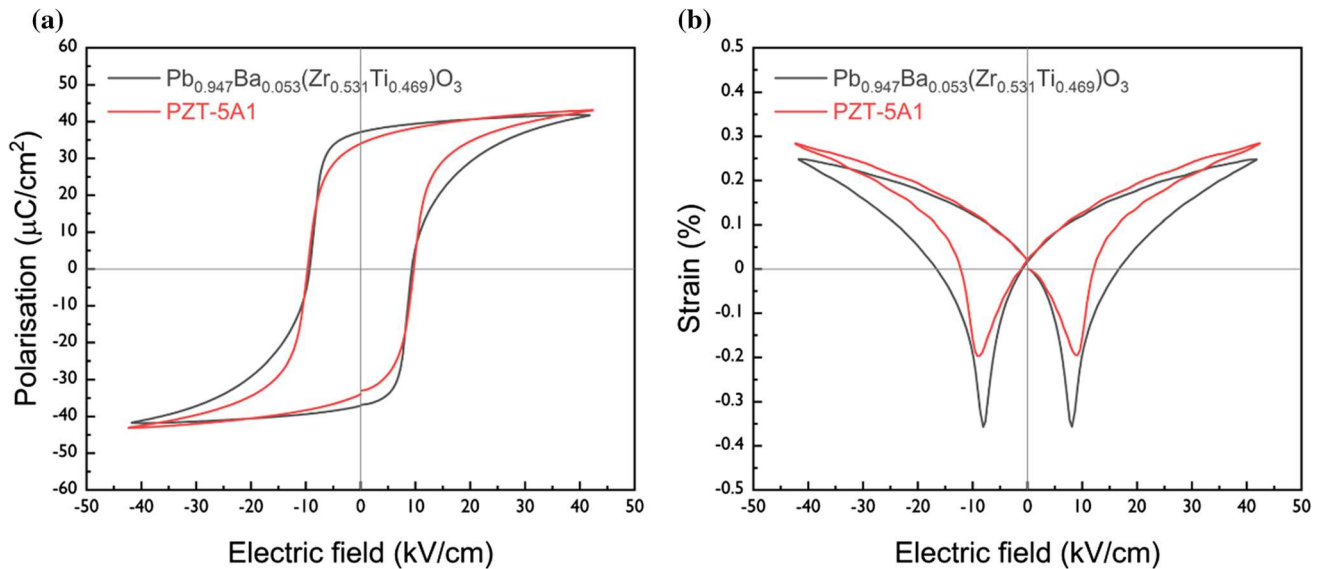
(a)

(b)

Figure 11 (**a**) Polarisation vs. electric field (P-E) hysteresis loops for $Pb_{0.947}Ba_{0.053}(Zr_{0.531}Ti_{0.469})O_3$ and PZT-5A1 variant, and (**b**) strain vs. electric field (S-E) hysteresis loops.
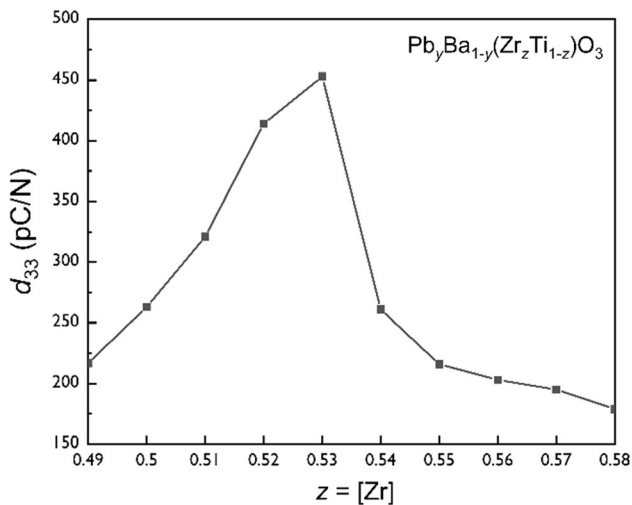

Figure 12 Berlincourt d_{33} coefficients for randomly oriented ceramics with Zr concentration $0.49 \leq z \leq 0.58$.

from tetragonal compositions towards the MPB, to a maximum $d_{33} = 453$ pC/N for $z = 0.53$, comparable to commercial 'soft' PZT compositions [37]. The enhanced d_{33} in randomly oriented ceramics with solid solution incorporation of 5 vol.% BaTiO$_3$ seeds with MPB-like compositions is ascribed to a lowering of the T_C, allowing for easier polarisation rotation and facilitating domain wall motion [38].

Conclusions

Proof of concept for the fabrication of 94% $[001]_c$ fibre-textured PZT ceramics was established using 5 vol.% BaTiO$_3$ seeds. Dissolution of BaTiO$_3$ into the PZT matrix resulted in a tetragonal structural shift away from the MPB region. Crystal structure characterisation and mapping of the temperature-sensitive phase transition behaviour of BaTiO$_3$-modified PZT ceramics indicated that the MPB region shifts slightly towards the rhombohedral side of the PZT phase space. A series of BaTiO$_3$-modified compositions of PZT ($Pb_yBa_{1-y}(Zr_zTi_{1-z})O_3$) was explored where the final Zr concentration ranged from $z = 0.49$ to $z = 0.58$. The dielectric, ferroelectric, and electromechanical behaviour of the modified compositional space was established to lay the groundwork for future developments focused on texturing PZT ceramics. An initial PZT matrix composition of $Pb(Zr_{0.56}Ti_{0.44})O_3$ resulted in an identified MPB composition of $Pb_{0.947}Ba_{0.053}(Zr_{0.531}Ti_{0.469})O_3$ exhibiting 'soft' PZT behaviour with a $d_{33} = 453$ pC/N similar to that of commercial PZT-5A1 with $d_{33} \sim 410$ pC/N and comparable polarisation/strain hysteresis data. This suggests that initial PZT matrix compositions with increased Zr:Ti ratios are desirable when compensating for the incorporation of BaTiO$_3$ seeds to ultimately achieve near MPB-like properties.

Acknowledgements

Declarations

Conflict of interests The authors declare that they have no known competing financial interests or personal relationships that could have appeared to influence the work reported in this paper.

Data availability The authors confirm that the data supporting the findings of this study are available within the article.

Ethical approval The authors confirm that the nature of the work did not require prior ethical approval by an institutional review board or equivalent ethics committee.

Supplementary information The authors confirm that there are no additional materials omitted from the main body.

References

[1] Shirane G, Takeda A (1952) Phase transitions in solid solutions of PbZrO$_3$ and PbTiO$_3$ (I) Small concentrations of PbTiO$_3$. J Phys Soc Jpn 7(1):5–11

[2] Shirane G, Suzuki K, Takeda A (1952) Phase transitions in solid solutions of PbZrO$_3$ and PbTiO$_3$ (II) X-ray study. J Phys Soc Jpn 7(1):12–18

[3] Shirane G, Suzuki K (1952) Crystal structure of Pb(Zr-Ti)O$_3$. J Phys Soc Jpn 7:333

[4] Sawaguchi E (1953) Ferroelectricity versus antiferroelectricty in the solid solution of PbZrO$_3$ and PbTiO$_3$. J Phys Soc Jpn 8(5):615–629

[5] Jaffe B, Roth RS, Marzullo S (1954) Piezoelectric properties of lead zirconate-lead titanate solid-solution ceramics. J Appl Phys 25:809–810

[6] Du X-H, Belegundu U, Uchino K (1997) Crystal orientation dependence of piezoelectric properties in lead zirconate titanate: theoretical expectation for thin films. Jpn J Appl Phys 36(9A):5580–5587

[7] Du X-H, Zheng J, Belegundu U, Uchino K (1998) Crystal orientation dependence of piezoelectric properties of lead zirconate titanate near the morphotropic phase boundary. Appl Phys Lett 72(19):2421–2423

[8] Noheda B, Cox DE, Shirane G, Gonzalo JA, Cross LE, Park S-E (1999) A monoclinic ferroelectric phase in the Pb(Zr$_{1-X}$Ti$_X$)O$_3$ solid solution. Appl Phys Lett 74(14):2059–2061

[9] Jaffe B, Cook WR Jr, Jaffe H (1971) Piezoelectric ceramics. Academic Press Inc, London

[10] Takahashi S (1982) Effects of impurity doping in lead zirconate-titanate ceramics. Ferroelectrics 41(1):143–156

[11] Zheng H, Reaney IM, Lee WE, Jones N, Thomas H (2002) Effects of octahedral tilting on the piezoelectric properties of strontium/barium/niobium-doped soft lead zirconate titanate ceramics. J Am Ceram Soc 85(9):2337–2344

[12] Carl K, Härdtl KH (1978) Electrical after-effects in Pb(Ti, Zr)O$_3$ ceramics. Ferroelectrics 17(1):473–486

[13] Kuwata J, Uchino K, Nomura S (1982) Dielectric and piezoelectric properties of 0.91Pb(Zn$_{1/3}$Nb$_{2/3}$)O$_3$–0.09PbTiO$_3$ single crystals. Jpn J Appl Phys 21(9):1298–1302

[14] Park S-E, Shrout TR (1997) Characteristics of relaxor-based piezoelectric single crystals for ultrasonic transducers. IEEE Trans Ultrason Ferroelectr Freq Control 44(5):1140–1147

[15] Zhang S, Lee S-M, Kim D-H, Lee H-Y, Shrout TR (2007) Temperature dependence of the dielectric, piezoelectric, and elastic constants for Pb(Mg$_{1/3}$Nb$_{2/3}$)O$_3$-PbZrO$_3$-PbTiO$_3$ piezocrystals. J Appl Phys 102:114103

[16] Hosono Y, Yamashita Y, Sakamoto H, Ichinose N (2003) Growth of single crystals of high-Curie-temperature Pb(In$_{1/2}$Nb$_{1/2}$)O$_3$-Pb(Mn$_{1/3}$Nb$_{2/3}$)O$_3$-PbTiO$_3$ ternary systems near morphotropic phase boundary. Jpn J Appl Phys 42(9A):5681–5686

[17] Poterala SF, Trolier-McKinstry S, Meyer RJ Jr, Messing GL (2011) Processing, texture quality, and piezoelectric properties of $<001>_c$ textured $(1–x)Pb(Mg_{1/3}Nb_{2/3})TiO_3-xPbTiO_3$ ceramics. J Appl Phys 110:014105

[18] Chang Y, Watson BH III, Fanton M, Meyer RJ Jr, Messing GL (2017) Enhanced texture evolution and piezoelectric properties in CuO-doped $Pb(In_{1/2}Nb_{1/2})O_3$-$Pb(Mg_{1/3}Nb_{2/3})O_3$-$PbTiO_3$ grain-oriented ceramics. Appl Phys Lett 111:232901

[19] Messing GL, Poterala SF, Chang Y, Frueh T, Kupp ER, Watson BH III, Walton RL, Brova MJ, Hofer A-K, Bermejo R, Meyer RJ Jr (2017) Texture-engineered ceramics-Property enhancements through crystallographic tailoring. J Mater Res 32:1–23

[20] Luo J, Hackenberger W, Zhang S, Shrout TR (2008) Elastic, Piezoelectric and dielectric properties of PIN-PMN-PT crystals grown by Bridgman method. IEEE Int Ultrason Symp 102:261–264

[21] Fushimi S, Ikeda T (1967) Phase equilibrium in the system $PbO-TiO_2-ZrO_2$. J Am Ceram Soc 50(3):129–132

[22] Clarke R, Whatmore RW, Glazer AM (1976) Growth and characterization of $PbZr_xTi_{1-x}O_3$ single crystals. Ferroelectrics 13(1):497–500

[23] Devemy S, Courtois C, Champagne P, Lippert M, Moreau G, Petit F, Leriche A (2009) Textured PZT ceramics. Powder Technol 190(1):141–145

[24] Muramatsu H, Kimura T (2004) Preparation of bulk $Pb(Zr, Ti)O_3$ with crystallographic texture by templated grain growth Method. J Electroceram 13:531–535

[25] Messing GL, Trolier-McKinstry S, Sabolsky EM, Duran C, Kwon S, Brahmaroutu B, Park P, Yilmaz H, Rehrig PW, Eitel KB, Suvaci E, Seabaugh M, Oh KS (2004) Templated grain growth of textured piezoelectric ceramics. Crit Rev Solid State Mater Sci 29(2):45–96

[26] Ikeda T (1959) Studies on $(Ba-Pb)(Ti-Zr)O_3$ system. J Phys Soc Jpn 14(2):168–174

[27] Zheng H, Reaney IM, Lee WE, Jones N, Thomas H (2002) Effects of octahedral tilting on the piezoelectric properties of Sr-doped lead zirconate titanate. Ferroelectrics 268(1):125–130

[28] Poterala S, Chang Y, Clark T, Meyer RJ Jr, Messing GL (2010) Mechanistic interpretation of the Aurivillius to perovskite topochemical microcrystal conversion process. Chem Mater 22:2061–2068

[29] Lotgering FK (1959) Topotactical reactions with ferrimagnetic oxides having hexagonal crystal structures-I. J Inorg Nucl Chem 9:249–254

[30] ASTM E112–13 (2013) Standard test methods for determining average grain size. ASTM International, West Conshohocken, PA

[31] Sabolsky EM, Messing GL, Trolier-McKinstry S (2001) Kinetics of templated grain growth of $0.65Pb(Mg_{1/3}Nb_{2/3})O_3 \bullet 0.35PbTiO_3$. J Am Ceram Soc 84(11):2507–2513

[32] Soares MR, Senos AMR, Mantas PQ (2000) Phase coexistence region and dielectric properties of PZT ceramics. J Eur Ceram Soc 20:321–334

[33] Budimir M, Damjanovic D, Setter N (2006) Piezoelectric response and free-energy instability in the perovskite crystals $BaTiO_3$, $PbTiO_3$, and $Pb(Zr, Ti)O_3$. Phys Rev B 73:174106

[34] Shannon RD, Prewitt CT (1969) Effective ionic radii in oxides and fluorides. Acta Cryst B25:925–946

[35] Li G, Haertling G (1995) Dielectric, ferroelectric and electric field-induced strain properties of $(Pb_{1-x}Ba_x)(Zr_{1-y}Ti_y)O_3$ ceramics. Ferroelectrics 166(1):31–45

[36] Zhang S, Shrout TR (2010) Relaxor-PT single crystals: observations and developments. IEEE Trans Ultrason Ferroelectr Freq Control 57(10):2138–2146

[37] MIL-STD-1376B (1995) Piezoelectric ceramic material and measurements guidelines for sonar transducers, U.S. Department of Defence

[38] Damjanovic D (2010) A morphotropic phase boundary system based on polarization rotation and polarization extension. Appl Phys Lett 97:062906